Selective Diffusion for Oriented Pattern Extraction: Application to Tagged Cardiac MRI Enhancement

A. Histace [a], M. Ménard [b] , C. Cavaro-Ménard [c]

[a] *ETIS UMR CNRS 8051, ENSEA/University of Cergy Pontoise, France*

[b] *L3i, Pôle Science et Technologie, University of La Rochelle, France*

[c] *LISA, University of Angers, France*

Corresponding author: aymeric.histace@ensea.fr

Abstract

Anisotropic regularization PDE's (Partial Differential Equation) raised a strong interest in the field of image processing. The benefit of PDE-based regularization methods lies in the ability to smooth data in a nonlinear way, allowing the preservation of important image features (contours, corners or other discontinuities). In this article, a selective diffusion approach based on the framework of Extreme Physical Information theory is presented. It is shown that this particular framework leads to a particular regularization PDE which makes the integration of prior knowledge possible within the diffusion scheme. As a proof of feasibility, results of oriented pattern extractions are first presented on ad hoc images and second on a particular medical application: Tagged cardiac MRI (Magnetic Resonance Imaging) enhancement.

Key words: Image Diffusion, Extreme Physical Information, Oriented Pattern Extraction, Selectivity, Tagged Cardiac MRI.

1 Introduction

Since the pioneering work of Perona-Malik [1], anisotropic regularization PDE's raised a strong interest in the field of image processing. The benefit of PDE-based regularization methods lies in the ability to smooth data in a nonlinear way, allowing the preservation of important image features (contours, corners or other discontinuities). Thus, many regularization schemes have been presented so far in the literature, particularly for the problem of scalar image restoration [1–12]. In [8] Deriche et *al.* propose a unique PDE to express the

whole principle: If we denote $\psi(\mathbf{r},0) : \mathbb{R}^2 \times \mathbb{R}^+ \rightarrow \mathbb{R}$ the intensity function of an image, to regularize the considered image is equivalent to a minimization problem of a particular PDE which can be seen as the superposition of two monodimensional heat equations, respectively oriented in the orthogonal direction of the gradient and in the tangential direction (Eq. (1) and Fig. 1) :

$$\frac{\partial \psi}{\partial t} = \frac{\phi'(\|\nabla\psi\|)}{\|\nabla\psi\|}\psi_{\xi\xi} + \phi''(\|\nabla\psi\|)\psi_{\eta\eta} \qquad , \tag{1}$$

where $\eta = \nabla\psi/\|\nabla\psi\|$ and $\xi \perp \eta$ and $\phi : \mathbb{R} \rightarrow \mathbb{R}$ is a decreasing function.

This PDE is characterized by an anisotropic diffusive effect in the privileged directions ξ and η allowing a denoising of a scalar image.

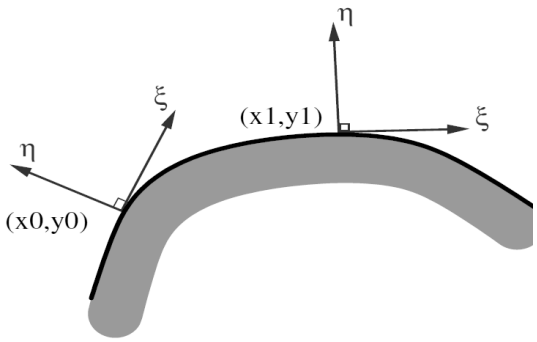

Fig. 1. An image contour and its moving vector basis (ξ, η). Taken from [11].

The major limitations of this diffusion process is its high dependance to the intrinsic quality of the original image, and the impossibility to integrate prior information on the pattern to be restored if it can be characterized by particular data (orientation for example). Moreover, no characterization of the uncertainty/inaccuracy compromise can be made on the studied pixel, since the time evolution parameter is not directly integrated in the minimization problem on which the common diffusion equations rely [13]. In particular applications, it can be a strong limitation as we will notice in section 2.

In this article, we propose an original PDE directly integrating the scale parameter, and allowing the taking into account of prior knowledge on the pattern to restore. We propose to use an original theory known as Extreme Physical Information (EPI) recently developed by Frieden [14], and applied to image processing by Courboulay et *al.* [15] to derive this PDE.

The second section of this article deals with the presentation of a possible practical medical application. The aim of this section is to demonstrate the validity of our approach. The third section deals with presentation of EPI and with the obtaining of the particular PDE that will be implemented. The fourth section presents a direct application to the presented diffusion process on ad hoc synthetic images. The Fifth section shows results of restoration

considering particular practical medical case of the second section. The last part is dedicated to discussion.

2 Practical medical application presentation: tagged cardiac MRI restoration

The non invasive assessment of the cardiac function is of major interest for the diagnosis and the treatment of cardiovascular pathologies. Whereas classical cardiac MRI only enables radiologists to measure anatomical and functional parameters of the myocardium (mass, volume...), tagged cardiac MRI makes the evaluation of local intra-myocardial displacements possible. For instance, this type of information can lead to a precise characterization of the myocardium viability after an infarction. Moreover, data concerning myocardium viability makes the decision of the therapy possible: Medical treatment, angiopathy, or coronary surgery and follow-up of the amelioration of the ventricular function after reperfusion.

The SPAMM (Space Modulation of Magnetization) acquisition protocol [16] we used for the tagging of MRI data, displays a deformable 45-degrees oriented dark grid which describes the contraction of myocardium (Fig. 2) on the images of temporal Short-Axis (SA) sequences. This is the temporal tracking of this grid that can enable radiologists to evaluate the local intramyocardial displacement.

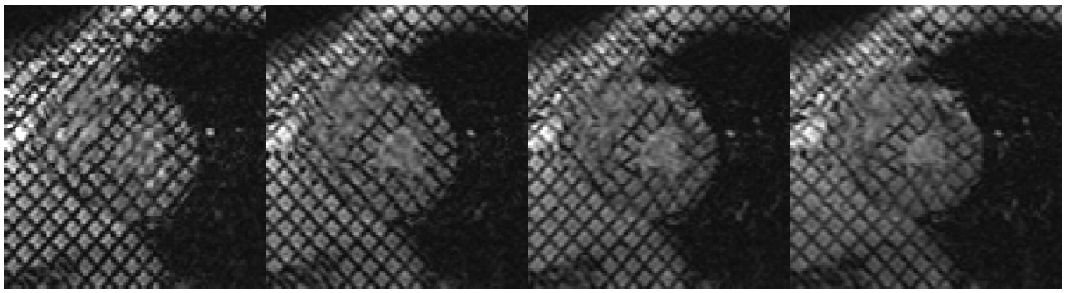

Fig. 2. SA tagged MRI of the Left Ventricle (LV) extracted from a sequence acquired between end-diastole and end-systole.

Nevertheless, tagged cardiac images present peculiar characteristics which make them difficult to analyze. More precisely, images are of low contrast compared with classical MRI, and their resolution is only of approximately one centimeter. Numerous studies were carried out concerning the analysis of the deformations of the grid of tag on SA sequences (see [17,18] for a complete overview), but all have in common the necessary enhancement of tagged cardiac images, and more precisely of the grid of tags in order to perform the corresponding tracking using, for instance, a grid of active contours. Since

no technique has allowed to develop a complete "Gold Standard" method, we propose to develop a diffusive restoration approach which will make the enhancement of the oriented grid of tags possible (Fig. 2). This non-linear smoothing will make the temporal segmentation of the grid using active contours possible.

This methodological choice is principally motivated by the fact that, in this particular framework, classical image enhancement techniques like Gabor filtering are not totally adapted to generate a potential map of the processed image, making the precise tracking of the grid possible, using parametric active contours, as shown in [19]. More precisely, if Gabor filtering makes a good regularization of the grid possible [23], it appears that the spatial localization of the regularized grid is not precise enough to obtain an accurate tracking of the grid thanks to parametric active contours. However, tracking the tags with such a parametric active contour grid is of primary interest in the framework of this application, since the corresponding classical mathematical modeling using B-splines allows to locally compute geometrical parameters, from which classical clinical parameters can be derived.

Classically, diffusive restoration approaches like the Perona-Malik's former one [1], perform a non-linear smoothing of the data by taking into consideration the local value of the gradient intensity. This makes the enhancement of the boundaries of the image possible. Nevertheless, as one can notice on Fig. 3, due to the fact that norms of the gradient levels of tagged MRI are very noisy, and then unadapted to classical restoration approaches, it is necessary to develop a method that integrates within diffusion process more than only this classical parameter: for instance, calculation and integration of the direction of local gradients of the grid could be of primary interest.

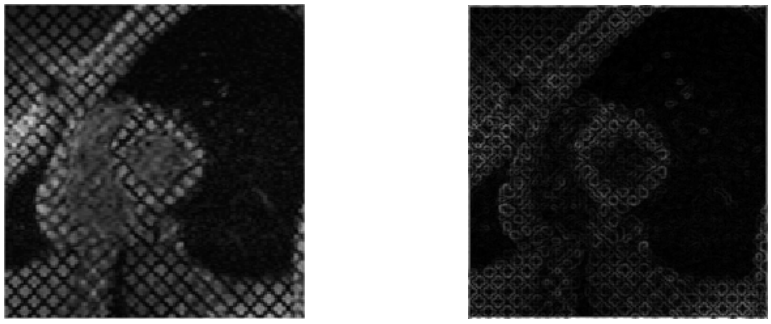

(a) (b)

Fig. 3. (a) Original Image, (b) Norm of the corresponding gradients. As one can notice, the grid of tags does not allow us to obtain a good gradient attractor for a good tracking of the grid.

This can be achieved by considering some variations of the classical restoration

approaches like, for example, a variant of the classical heat equation process given by

$$\frac{\partial \psi}{\partial t} = C(||A.\nabla\psi||)\triangle\psi, \tag{2}$$

or by a variant of the Perona-Malik's process [1] given by

$$\frac{\partial \psi}{\partial t} = div(C(||\mathbf{A}.\nabla\psi||)\nabla\psi) \ . \tag{3}$$

For both Eqs (2) and (3), $C(u) = e^{-\frac{u^2}{\lambda}}$ and $\mathbf{A}$ is a vector field defining the particular direction(s) to preserve from the diffusion process (in this particular medical application, the gradient direction of the grid). λ represents here a soft threshold driving the decrease of $C(.)$. In both cases, the directional weighting of the diffusion process is driven by the scalar product between the norm of the local gradient and $\mathbf{A}$. As a consequence when local gradient and $\mathbf{A}$ are parallel, there is no diffusion, for $C(||\mathbf{A}.\nabla\psi|| = 0$, whereas all other directions are diffused: the grid of tags is enhanced.

Nevertheless, like in all classical diffusion approaches (see references in the introduction section), these two solutions do not make the integration of the evolution parameter t (or scale parameter) possible, since corresponding functional to minimize does not integrate it fundamentally, as we previously noticed it.

Moreover, if particular information theories are often used to stop diffusion process at optimal value of evolution parameter ([7] for instance), the derived PDE is not directly issued from this chosen information theory. As a consequence, the possibility to optimize uncertainty/inaccuracy compromise during restoration processes is lost.

That is why we propose, in the following, an adapted restoration process derived directly from a particular information theory known as EPI, which directly integrates the time evolution parameter. Concrete results on a particular presented medical application, which is presented at the end of the article.

3 EPI and image diffusion

3.1 EPI

Developed by Frieden, the principle of Extreme Physical Information (EPI) is aimed at defining a new theory of measure. The key element of this new theory is that it takes into account the effect of an observer on a measure scenario. As stated by Frieden [20,14], "EPI is an observer-based theory of physics". By observing, the observer is both a collector of data and an interference that affects the physical phenomenon which produces the data. Although the EPI principle brings new concepts, it still has to rest on the definition of information. Fisher information was chosen for its ability to effectively represent the quality of a measure. Fisher information measurement was introduced by Fisher in 1922 [21] in the context of statistical estimation. In the last ten years, a growing interest for this information measurement has arisen in theoretical physics. In his recent book [14], Frieden has characterized Fisher information measurement as a versatile tool to describe the evolution laws of physical systems; one of his major results is that the classical evolution equations as the Schrödinger wave equation, the Klein-Gordon equation, the Helmotz wave equation, or the diffusion equation, can be derived from the minimization of Fisher information measurement under proper constraint.

3.2 Shannon entropy and Fisher information

In the following, we consider a random variable X whose probability density function is denoted as $p_X(x)$. Its Shannon entropy writes

$$H_S(X) = -\int p_X(x)\log(p_X(x))dx \qquad , \tag{4}$$

and its Fisher information measurement writes

$$I(X) = \int \left(\frac{\partial p_X(x)}{\partial x}\right)^2 \frac{dx}{p_X(x)} \qquad . \tag{5}$$

The analytic properties of the two information measurements are quite different. Thus, whereas H_S is a *global* measurement of smoothness in $p_X(x)$, I is a *local* measurement. Hence, when minimized through variation of $p_X(x)$, Fisher's form gives a differential equation while Shannon's always gives directly the same form of solution, an exponential function [14].

Moreover, assuming that Shannon entropy is a particular case of the Kullback-Leibler cross entropy H_{KL} given by

$$H_{KL}(X,R) = \int p_X(x) \log\left(\frac{p_X(x)}{p_R(x)}\right) \quad , \tag{6}$$

with $p_R(x)$ a reference probability density function, I can be related to H_{KL} as follows [14]:

$$I(X) = -\frac{2}{\triangle x^2} H_{KL}(X, X_{\triangle x}) \quad , \tag{7}$$

where $X_{\triangle x}$ is a random variable whose probability density function is $p_X(x + \triangle x)$. This result is very interesting for the characterization of the diffusion process as we will see later.

3.3 EPI and image diffusion

Practically speaking, the EPI principle can be seen as an optimization of the information transfer from the system under measurement to the observer, each one being characterized by a Fisher Information measure denoted, respectively, I and J. The first one is representative of the quality of the estimation of the data, and the second one allows to take into account the effect of the subjectivity of the observer on the measurement. The existence of this transfer leads to create fluctuations on the acquired data compared to the real ones. In fact, this information channel leads to the loss of accuracy on the measurement whereas the certainty is increased.

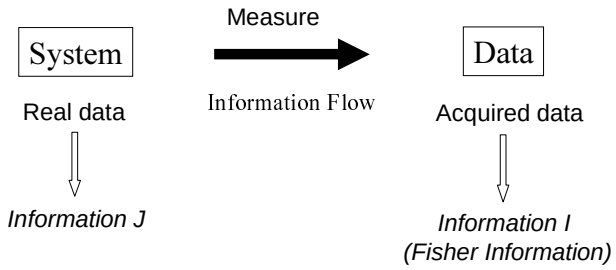

Fig. 4. Fisher Information

The goal of EPI is then to minimize the difference $I - J$ (*i.e.* the uncertainty/inaccurracy compromise) denoted K, called the Physical Information of the system, in order to optimize the information flow.

Application to image diffusion can be illustrated by Fig. 5.

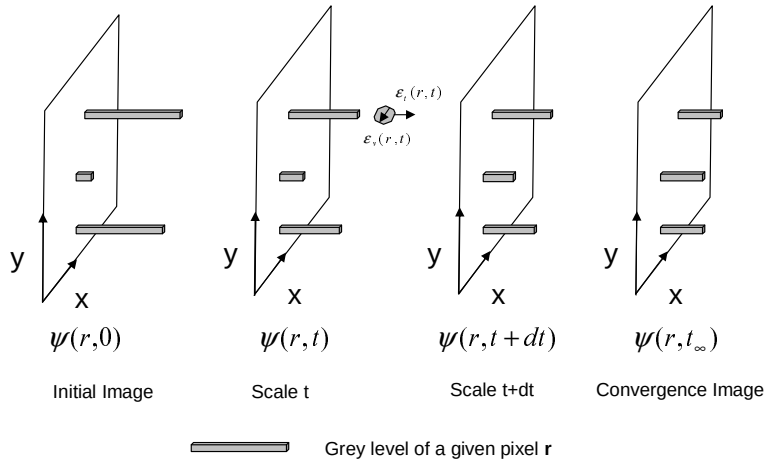

Fig. 5. Uncertainty/inaccuracy compromise and isotropic image diffusion. When parameter $t \to \infty$, luminance of all pixels of the corresponding image is the same, and equal to the spatial average of the initial image.

In this case, we will consider that X is equal to $\psi(\mathbf{r}, t)$, the luminance function characterizing the processed image. As far as isotropic image diffusion is concerned, the uncertainty deals with the fluctuations of the grey level of a given pixel compared with its real value, whereas the inaccuracy deals with the fluctuations of the spatial localization of a given pixel compared with the real one. The two different errors ($\varepsilon_r(t)$ and $\varepsilon_v(t)$) of Fig. (5), which are introduced all along the diffusion process, are characterized by a measurement of Fisher information (Eq. (7)). Intrinsic Fisher information J will be an integration of the diffusion constraints we impose on the processing.

Then, we can apply EPI to image diffusion process by considering an image as a measurement of characteristics (luminance, brightness, contrast) of a particular scene, and diffusion as the observer of this measurement at a given scale or a given time parameter. Extreme Physical Information K is then defined as follows [14,19,22]:

$$K(\psi) = \int\int d\Omega dt \times \left[(\nabla - \mathbf{A})\,(\nabla - \mathbf{A})\,\psi^2 + (\frac{\partial \psi}{\partial t})^2 - \psi^2 \right] , \tag{8}$$

where $\psi(\mathbf{r}, 0) : \mathbb{R}^2 \times \mathbb{R}^+ \to \mathbb{R}$ is the luminance function of the original image, and $\mathbf{A}$ a potential vector representing the parameterizable constraint(s) integrated within diffusion process (see also Eqs (2) and (3)).

Extremizing K by Lagrangian approach leads to a particular diffusion equation given by (see [14] for more details on the calculation itself) :

$$\frac{\partial \psi}{\partial t} = \frac{1}{2}(\nabla - \mathbf{A}).(\nabla - \mathbf{A})\psi \qquad . \tag{9}$$

As a consequence, the possible parameterization of **A**, makes the taking into account of particular characterized patterns possible in order to preserve them from the diffusion process.

3.4 About ***A***

The **A** potential allows to control the diffusion process, and introduces some prior constraints during image evolution. For instance, if no constraint are to be taken into account, we set **A** as vector null and Eq. (9) becomes :

$$\frac{\partial \psi}{\partial t} = \nabla . \nabla \psi = \triangle \psi \qquad . \tag{10}$$

which is the well known heat equation, characterized by an isotropic smoothing of the processed data.

In order to enlarge the possibility given by Eq. (9), the choice we make for **A** is based on the fact that Eq. (9) allows a weighting of the diffusion process with the difference of orientation between the local calculated gradient, and **A**. More precisely, to explain the way **A** is practically implemented, let us consider Fig. 6.

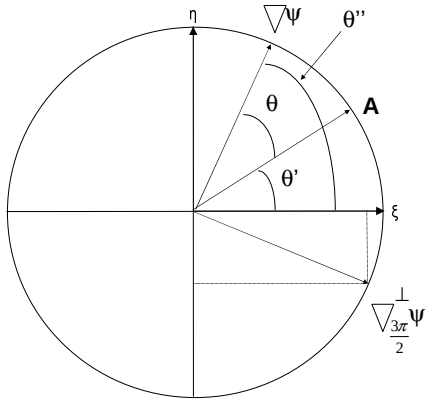

Fig. 6. Local geometrical implementation of **A** in terms of the local gradient $\nabla\psi$.

The expression of the local gradient $\nabla\psi$ in terms of θ" is, considering Fig. 6:

$$\nabla\psi = \begin{pmatrix} \|\nabla\psi\| \cos\theta'' \\ \\ \|\nabla\psi\| \sin\theta'' \end{pmatrix} , \tag{11}$$

and an expression of $\mathbf{A}$ in terms of θ', and the norm of $\nabla\psi$ is:

$$\mathbf{A}\psi = \begin{pmatrix} \|\nabla\psi\| \cos\theta' \\ \\ \|\nabla\psi\| \sin\theta' \end{pmatrix} . \tag{12}$$

The norm of $\mathbf{A}$ is imposed in order to make the comparison with the gradients possible. To this point, the most interesting expression of $\mathbf{A}$ would be the one in terms of θ which represents the difference angle between $\mathbf{A}$, and the local gradient. If we made so, using trigonometrical properties and noticing that $\theta = |\theta'' - \theta'|$, we obtain a new expression for $\mathbf{A}$:

$$\mathbf{A}\psi = \begin{pmatrix} \|\nabla\psi\|(\cos\theta'' \cos\theta + \sin\theta'' \sin\theta) \\ \\ \|\nabla\psi\|(\sin\theta'' \cos\theta - \cos\theta'' \sin\theta) \end{pmatrix} . \tag{13}$$

Eq. (13) could be simplified by integrating the vectorial expression of the local gradient (Eq. (11)):

$$\mathbf{A}\psi = \nabla\psi . \cos\theta + \nabla^{\perp}_{\frac{3\pi}{2}}\psi . \sin\theta \, . \tag{14}$$

with $\nabla^{\perp}_{\frac{3\pi}{2}}$ defined in Fig. 6.

From Eq. (14), we could then derive a general expression for $\mathbf{A}$ considering it as a vectorial operator :

$$\mathbf{A} : \psi \mapsto \mathbf{A}\psi = \nabla . \cos\theta + \nabla^{\perp}_{\frac{3\pi}{2}} . \sin\theta \, , \tag{15}$$

with θ the relative angle between $\mathbf{A}$ and $\nabla\psi$ for a given pixel and $\nabla^{\perp}$ the local vector orthogonal to ∇ (Fig. 6). This expression only represents the way it is possible to reformulate $\mathbf{A}$ by an orthogonal projection in the local base. Considering it, Eq. (9) becomes :

$$\frac{\partial\psi}{\partial t} = \frac{\partial^2\psi}{\partial\eta^2}.(1 - \cos\theta) + \frac{\partial^2\psi}{\partial\xi^2}.(1 - \cos\theta) \qquad . \tag{16}$$

One can notice on Eq. (16) that when the angle $\theta$is equal to 0 (*i.e.* $\mathbf{A}$ and $\nabla\psi$ are colinear), the studied pixel will not be diffused, since $\frac{\partial\psi}{\partial t} = 0$. On the contrary, a non-zero value of θ will lead to a weighted diffusion of the considered neighborhood of the pixel (Eq. (16)). As a consequence, by imposing local θ

values, it is possible to preserve particular patterns from the diffusive effect within restored image.

To this point, one major difference must be noticed among diffusion processes of Eqs. (2), (3) and (16): considering the latter, it is possible to select only one precise orientation of the local gradient not to be diffused thanks a judicious choice of θ'. This is not possible with Eqs. (2) and (3) as far as diffusion process is led by a scalar product between $\mathbf{A}$ and $\nabla\psi$.

4 Application to the extraction of oriented patterns

In this section, we present some results obtained on some simple images, in order to show the restoration and the denoising potential of the method. It is important to keep in mind that the following images have been chosen in accordance with the tagged MRI enhancement application which remains our main objective.

For practical numerical implementation, the process of Eq. (16) is discretized with a time step τ. The images $\psi(t_n)$ are calculated, with Eq. (16), at discrete instant $t_n = n\tau$ with n the number of iterations of the process.

First, let us consider an image showing vertical, horizontal, and 45°-oriented dark stripes on a uniform background (Fig. 7).

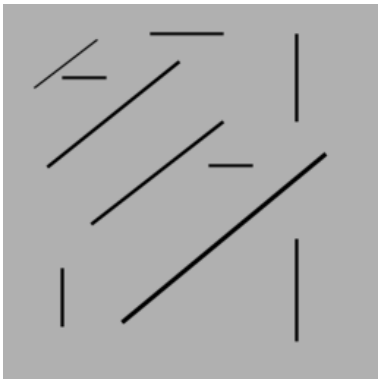

Fig. 7. Image 1: Dark stripes with various orientations on a uniform background.

Considering Eq. (16), by imposing two possible orientations for $\mathbf{A}$ (135°, 315°), which corresponds to the gradient orientations of the diagonal stripes, one could expect to preserve them from isotropic diffusion. Diffusion results are presented Fig. 8.

As expected, the vertical and horizontal dark stripes, within diffused images,

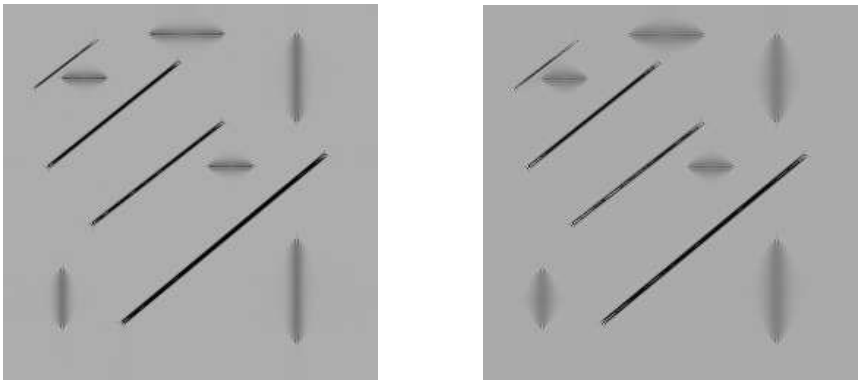

(a) (b)

Fig. 8. Diffusion of "Image 1" (Fig. 7) for (a) n=100 and (b) n=200. **A** is chosen in order to preserve only the diagonal stripes from the isotropic diffusion process. The time step τ is fixed to 0.2.

tend to disappear whereas the diagonal stripes are preserved all along the diffusion process.

Let us now consider a noisy simple grid diagonally oriented, and corrupted by a Gaussian noise of standard deviation set to 0.3.

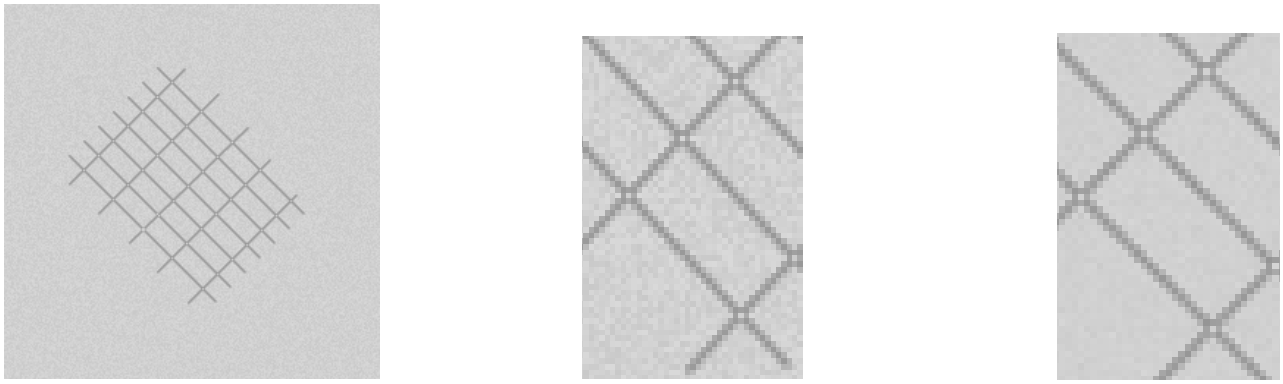

(a) (b) (c)

Fig. 9. Image 2: (a) Noisy diagonally oriented grid (Gaussian noise). PSNR (calculated with the non corrupted version of the grid as reference) is equal to 68 dB, (b) Zoom on a particular ROI of (a), (c) Diffusion of (a) for n=50. As one can notice, the grid itself is preserved from the diffusive effect of Eq. (9) whereas noise is progressively removed. Time step τ is fixed to 0.2.

To restore the grid without altering the corresponding boundaries, instead of imposing four orientations for **A**, which correspond to the four possible gradient orientations of the grid, we propose to extract this prior directional information by performing a Gabor filtering on the original corrupted image to extract the four main orientations. The entire process will be more detailed in

the next section. Now, if we apply the same diffusion process of Eq. (16) to this noisy simple grid, one can notice the denoising effect of the diffusion process (Fig. 9). As intended, the grid itself is not diffused at all and the increase of the Peak Signal to Noise Ratio (PSNR) from 68 dB to 84 dB, shows that the added Gaussian noise is progressively removed.

After the presentation of these first results on synthetic ad hoc images, we now present results obtained on the particular medical application presented: Enhancement of tagged cardiac MRI.

5 Application to the enhancement of tagged cardiac MRI

5.1 Processing

Considering Fig. 2, and Eq. (16), a solution to the problem of the enhancement of the grid of tags would have been to impose particular orientations for $\mathbf{A}$, considering the fact that the gradients to be preserved are well known and correspond to the orientations of the grid-of-tag ones (45°, 135°, 225°, 315°). However, because the contraction of the LV induces a deformation of the tags, the local orientation of the grid, at a time t, different from the initial one, can be no more characterized by imposed particular orientations. Moreover, because of the poor quality of MRI sequences, it appears that a calculation of the local orientation of $\mathbf{A}$, directly made on cardiac tagged images, would be strongly corrupted by noise.

As a consequence, we propose again to make this local estimation of the direction of $\mathbf{A}$ by performing a Gabor filtering. More precisely, this filtering is performed in the Fourier's domain, using the principle developed in [23,24] (Fig. 10).

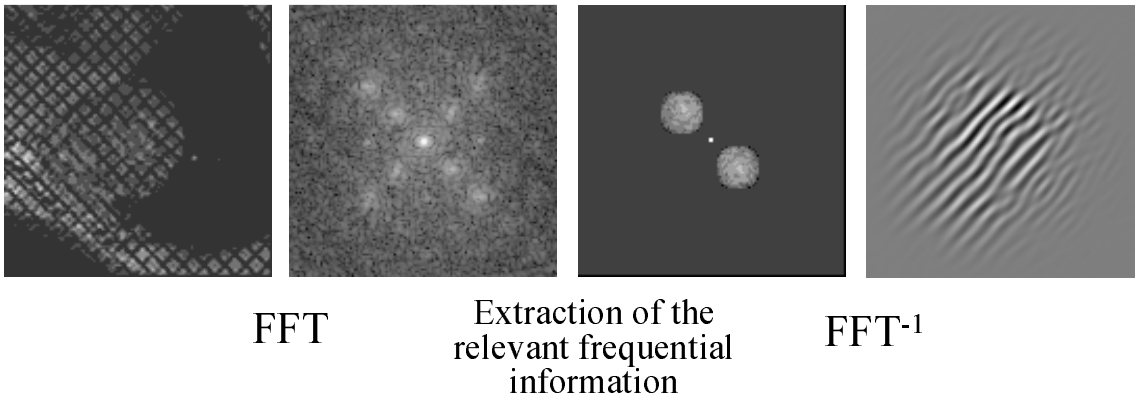

Fig. 10. Extraction of the tag information in the Fourier's domain.

This approach allows a denoising of the tag information which leads us to a more precise estimation of $\mathbf{A}$, and allows to take into account the deformations of the grid due to the contraction of the LV. In order to compute a precise estimation of θ angle of Eq. (16, we propose to directly use the method of Rao [25] and Terebes [10].

5.2 Results

The result presented in Fig. 11.a, shows the restoration of the 45°-oriented tag on the first image of a tagged cardiac sequence by the diffusion approach of Eq. (9). The step size chosen is 0.2. The iteration number is 80 [1]

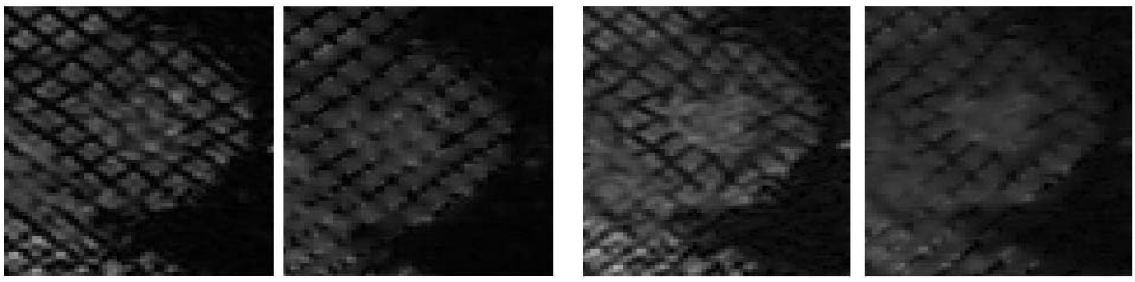

Fig. 11. Preservation of the 45°-oriented tag on (a) the initial image of a tagged sequence and (b) for $t \neq t_0$.

As we can see in Fig. 11.a, the diffusion process makes the fading of noisy artifacts possible , and non-45°-oriented lines.

Moreover, because orientation of $\mathbf{A}$ is locally calculated taking into account a particular neighborhood, the diffusion process remains efficient even if the tag is locally deformed due to myocardial contraction (Fig. 11.b).

At last, the enhancement effect of the selective diffusive process can also be seen on grey-level intensity evolution of a particular profile, extracted from original and enhanced tagged cardiac images. Fig. 12 shows that selectiveness of Eq. (9) makes the smoothing of all data except tag profiles possible.

[1] This number has been chosen in accordance with a quantitative study involving a comparison of automatic detection of the tags on restored image, with a manual expert segmentation. This quantitative study is presented in the next subsection.

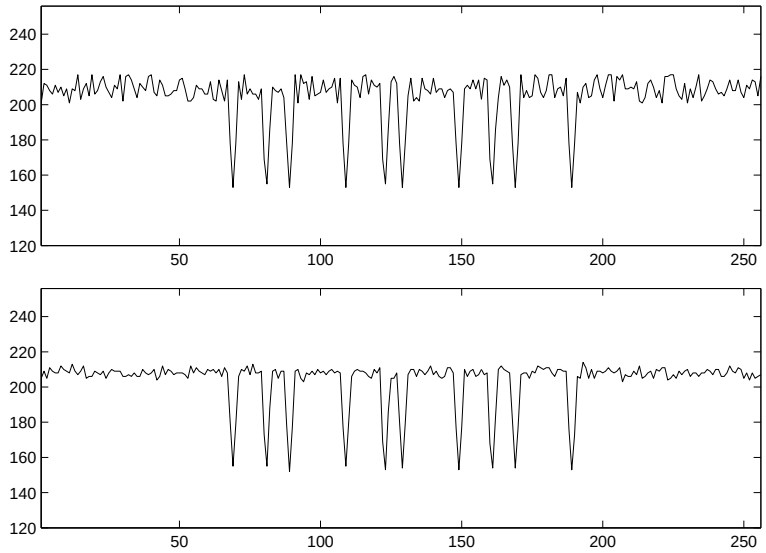

Fig. 12. **Up :** Original intensity profile extracted from an original tagged cardiac MRI (orthogonally to orientation of the grid of tags). **Bottom :** Enhanced image thanks to the process of Eq. (9) with the parametrization presented in previous subsection. x-axis represents the pixel position of the profile, y-axis represents the intensity value of the corresponding pixel. As one can notice, selectiveness of Eq. (9) makes the smoothing of all data except tag profiles possible.

5.3 Quantitative comparisons with classical PDE-based restoration approaches

Now, in order to evaluate the performance of the proposed restoration approach for the enhancement of tagged cardiac MRI, we propose to quantitatively compare it with classical PDE-based restoration methods. This quantitative study is mainly divided into 3 steps :

(1) First, a radiologist is asked to manually segment the tag of the LV Region of Interest (see Fig. 13 for visual illustration).
(2) Second, after having restored each tagged MR images of the same database used by the radiologist, using the considered diffusive method, a classical valley detection is performed in order to detect the "tag" pixels (see Fig. 14 for visual illustration). Mainly, this method is based on some local curvature detections computed on the restored tagged cardiac MR images. A large bibliography concerning local curvature detections can be found in [26]. For our purpose, this detection is obtained through the local calculation of the Hessian matrix eigenvalues locally computed. A classification of the local eigenvalues allows to only keep the pixels belonging to valleys, *i.e.* the tags.
(3) Third, each detected "tag" pixel is compared with the manual detected ones, and True Positive ratio as False Positive one is then computed. In order to only take into account pixels within myocardium (Fig. 13), the

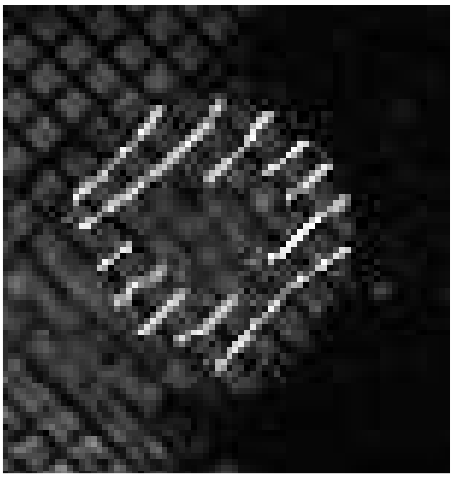

Fig. 13. Manual detection of the 45-degrees oriented tags on the LV Region of Interest

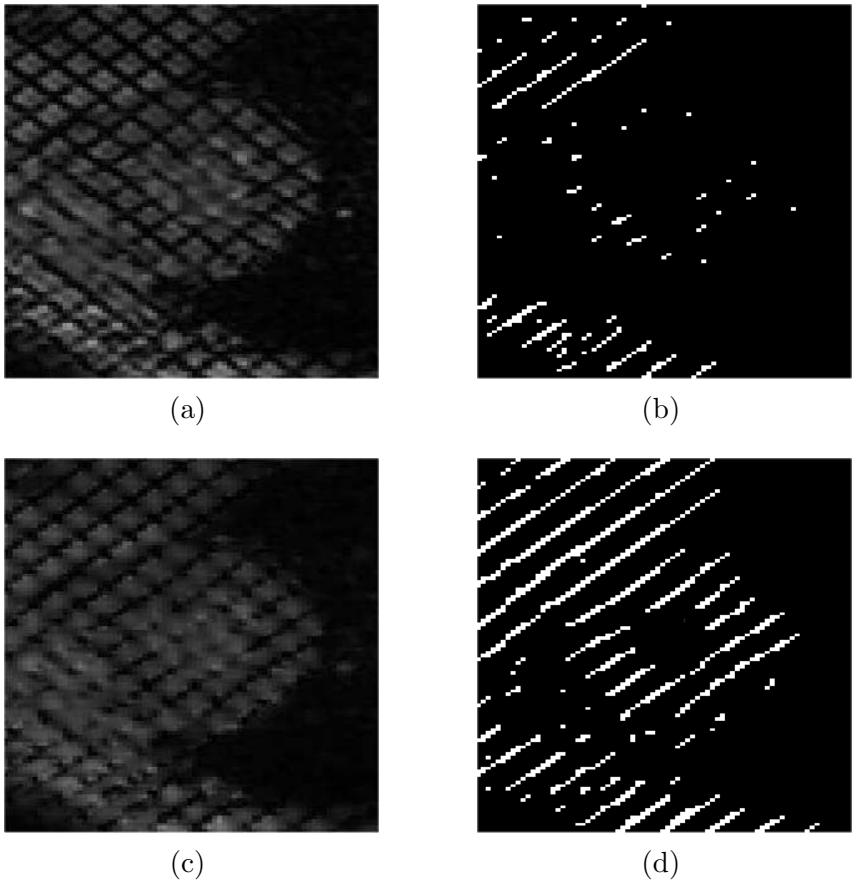

(a) (b)

(c) (d)

Fig. 14. Detections of valley on the original image and on the diffused one, using our approach. (a) Original image, (b) detection of valleys computed on (a), (c) restored image, (d) detection of valley computed (c).

corresponding Region of Interest is automatically computed thanks to an original segmentation of the epicardial and the endocardial boundaries on tagged cardiac MRI, proposed in [27].

The second, and the third step are computed for each iteration number of the diffusive process considered. For this quantitative study, four classical methods are compared : the proposed approach, the classical Heat Equation, the Perona-Malik's [1] approach and finally, the Weickert's [28] approach. Quantitative estimations have been computed on 30 tagged cardiac MRI (10 diastole, 10 mid-systole, 10 systole). Results are shown Fig. 15.

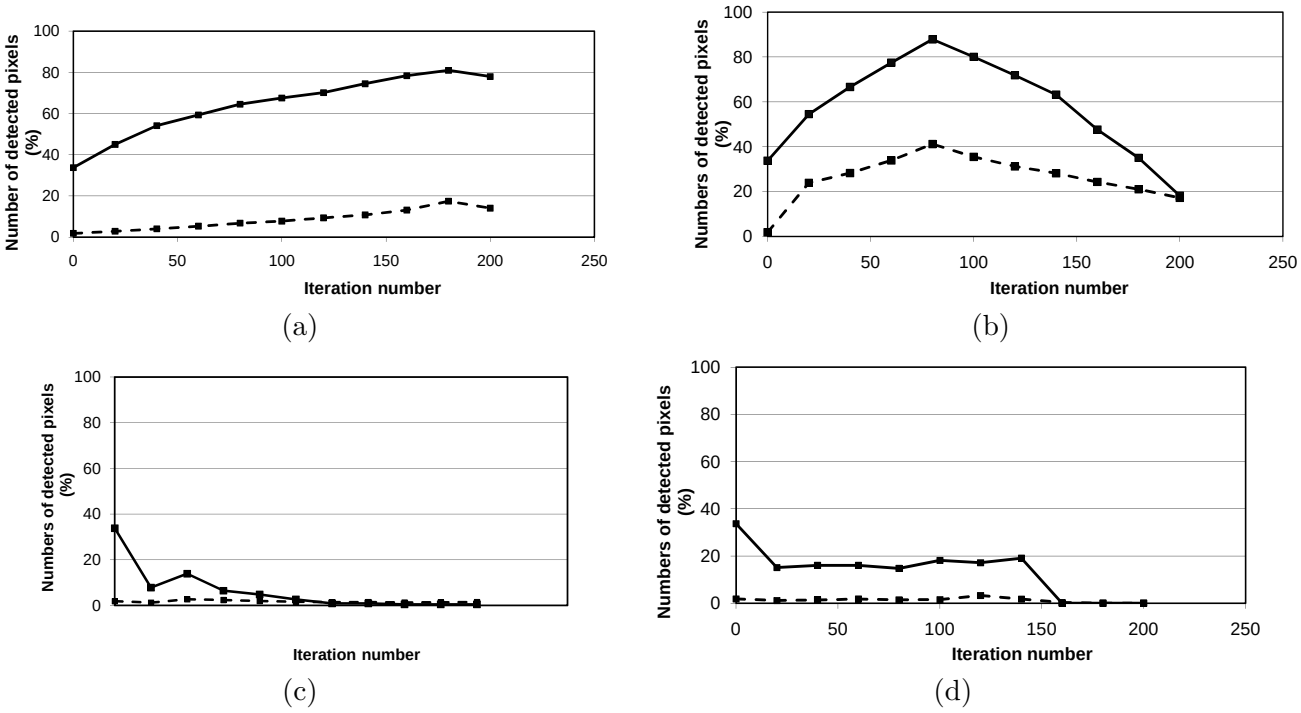

Fig. 15. Comparisons of the detected numbers of "tag" pixels function of diffusive iteration number among different image restoration approaches. (a) The proposed method, (b) the classical heat equation, (c) the Perona-Malik's approach [1], and finally (d), the Weickert's approach [28]. For each plot, solid line stands for True Positive "tag" pixels, and dash line for False Negative "tag" pixels.

Fig. 15.a shows that quantitatively, the number of detected "tag" pixels increases with the iteration number of the proposed restoration approach to finally reach a maximum of 80%. One can also notice that this increase is characterized by a smaller increase of the FP "tag" pixels, which is of primary importance from a clinical point of view (only 18% of FP "tagged" pixels correspond to the 80% of TP ones). This can be compared to the 90% of TP

"tag" pixels optimally detected using classical Heat Equation. This percentage is higher but is to be put in parallel with the corresponding 40% of FP pixels (Fig. 15.b). This high ratio can be explained by the fact that mathematically, a tag profile can be modeled by a Gaussian of standard deviation σ. As a consequence, we can suppose that the optimal result is nearly obtained when diffusive step t verifies $\sigma = \sqrt{2t}$. Nevertheless, ratio of FP "tag" pixels is too important to allow consideration of Heat Equation approach. Concerning now Figs. 15.c and .d, corresponding quantitative estimations of TP and FP "tag" pixels show that Perona-Malik's approach and Weickert's approach are not adapted to the tagged MRI restoration problem, since both ratios remains of low values for each step of the processes.

Finally this quantitative study tends to reinforce the visual impression given by Fig.11 and shows that the proposed approach leads to more adapted results than classical approaches.

5.4 Tracking of the grid of tags

In this section, we present a tracking of the grid of tags using a grid of parametric active contours. The corresponding potential map driving the displacements of the active grid has been performed using the proposed diffusive restoration approach.

Moreover, the tracking method, integrates the proposed restoration approach for the computation of the potential map, has been quantitatively compared to the same approach but in which the potential map is performed using classical Gabor filtering. Mainly, each approach is evaluated by its sensibility to the weighting parameters $w_{internal}$ and $w_{external}$ of the active grid, thanks to a measurement of the ratio of badly detected pixels within the whole active grid. Fig. 18 shows results of this quantitative comparison performed on five different sequences, each acquired at a different slice level of the LV (from base to apex [2]).

This quantitative study shows that for the proposed approach a 20% variation of the $w_{internal}$ and $w_{external}$ ration does not alter significantly the precision of the detected grid (only 10% of the corresponding pixels are badly detected) whereas a 10% variation of the ratio leads to a average global behavior of 20% for the method integrated with Gabor filtering.

[2] LV can be roughly represented by a pyramid with a base and a top called "apex".

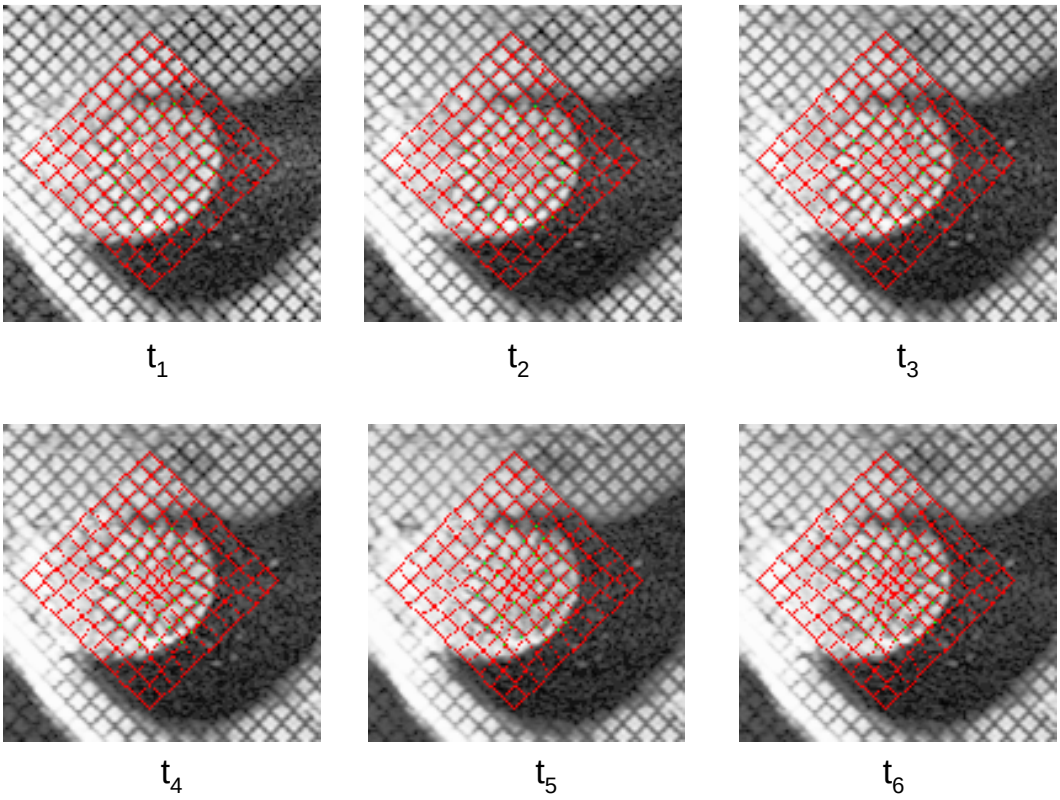

Fig. 16. Detection and tracking of the tagging grid on a SA sequence from diastole (t_1) to end systole (t_6).

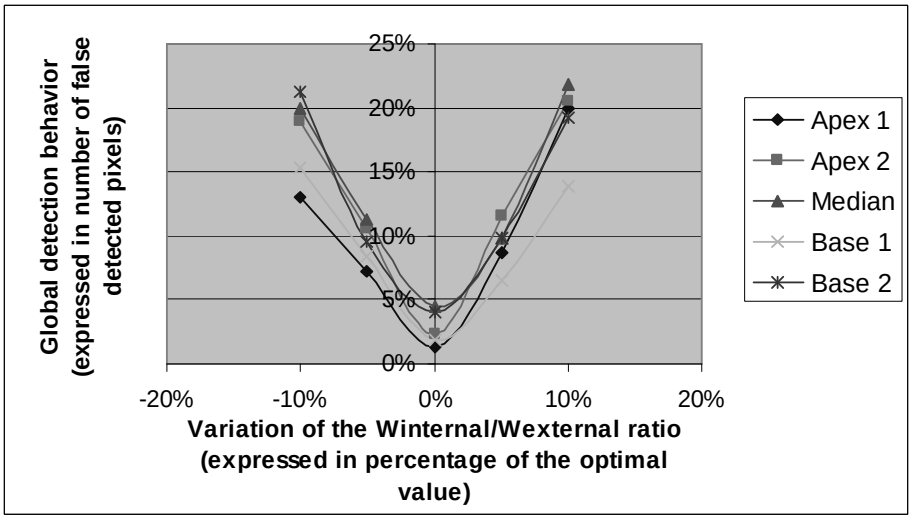

Fig. 17. Evolution of the global behavior of detection in terms of the $\frac{w_{internal}}{w_{external}}$ ratio for the Gabor filtering approach.

6 DISCUSSION

In this article an original diffusion method, based on the utilization of a particular PDE (Eq. (9)), derived from EPI theory, and directly integrating time

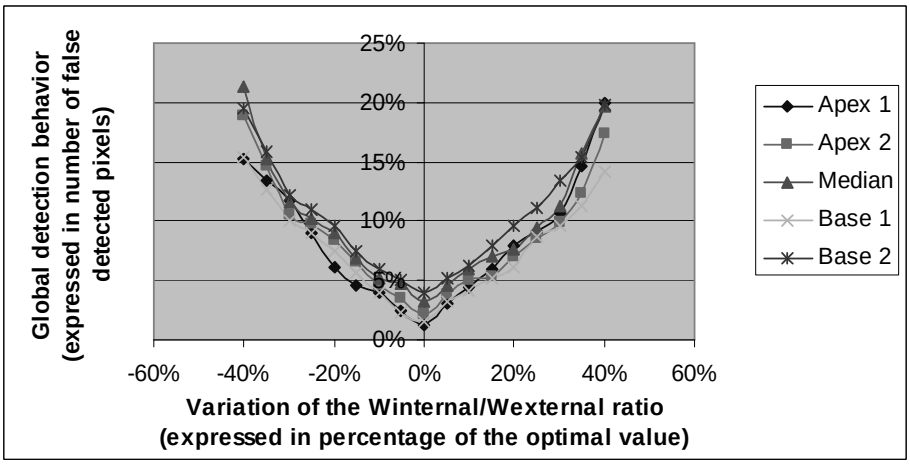

Fig. 18. Variation of the committed error on the detection of the grid of tags in terms of $\frac{w_{internal}}{w_{external}}$ ratio corresponding to the integration of the proposed restoration approach within the tracking process.

evolution parameter in its formulation, has been presented. It has been shown that the integration of the potential vector $\mathbf{A}$ within the formulation of this PDE makes the integration within the diffusion scheme of particular constraints possible. This has been assimilated to integration of selectiveness within classical isotropic diffusion process. Some examples on some ad hoc images have been presented to show the potential of the presented method in the areas of image denoising and extraction of oriented patterns. A particular application has also been proposed in the case of enhancement of tagged cardiac MRI, for which interesting results have been obtained, both visually and quantitatively. It has been demonstrated, as a proof of feasibility, that the developed approach may find applicability for the extraction of oriented patterns, which is still an open problem in many different areas of application like medical ones for instance. Moreover, because $\mathbf{A}$ is defined as a potential vector, one can easily imagine an extension of this work for vector-valued image regularization.

References

[1] P. Perona, J. Malik, Scale-space and edge detection using anistropic diffusion, IEEE Transcations on Pattern Analysis and Machine Intelligence 12 (7) (1990) 629–639.

[2] L. Alvarez, F. Guichard, P. Lions, J. Morel, Image selective smoothing and edge detection by nonlinear diffusion (ii), Arch. Rationnal Mech. Anal. 29 (3) (1992) 845–866.

[3] F. Catté, T. Coll, P. Lions, J. Morel, Image selective smoothing and edge detection by nonlinear diffusion, SIAM Journal of Applied Mathematics 29 (1)

(1992) 182–193.

[4] S. Geman, G. Reynolds, Constrained restoration and the recovery of discontinuities, IEEE Transactions on Pattern Analysis and Machine Intelligence 14 (3) (1992) 367–383.

[5] M. Nitzberg, T. Shiota, Nonlinear image filtering with edge and corner enhancement, IEEE Transactions on Pattern Analysis and Machine Intelligence 14 (8) (1992) 826–833.

[6] R. Whitaker, S. Pizer, A multi-scale approach to nonuniform diffusion, CVGIP:Image Understanding 57 (1) (1993) 99–110.

[7] J. Weickert, Multiscale texture enhancement, in: Computer Analysis of Images and Patterns, 1995, pp. 230–237.

[8] R. Deriche, O. Faugeras, Les EDP en traitements des images et visions par ordinateur, Traitement du Signal 13 (6) (1996) 551–578.

[9] J. Weickert, Anisotropic diffusion in image processing, Teubner-Verlag, Stuttgart, 1998.

[10] M. Terebes, R. Lavialle, Mixed anisotropic diffusion, in: Proceedings of the 16th International Conference on Pattern Recognition, Vol. 3, 2002, pp. 30760.

[11] D. Tshumperlé, R. Deriche, Diffusion PDEs on vector-valued images, Signal Processing Magazine, IEEE 19 (5) (2002) 16–25.

[12] D. Tschumperlé, R. Deriche, Vector-valued image regularization with PDE's: A common framework for different applications., IEEE Transactions on Pattern Analysis and Machine Intelligence 27 (2005) 506–517.

[13] N. Nordstrøm, Biased anisotropic diffusion-a unified regularization and diffusion approach to edge detection, Image and Vision Computing 8 (4) (1990) 318–327.

[14] B. Frieden, Physics from Fisher Information, Cambridge University Press, 1998.

[15] V. Courboulay, M. Ménard, M. Eboueya, P. Courtellemont, Une nouvelle approche du filtrage linaire optimal dans le cadre de l'information physique extrême, in proceedings of RFIA conference, 2002, pp. 897–905.

[16] E. Zerhouni, D. Parish, W. Rogers, A. Yang, E. Shapiro, Human heart : tagging with MR imaging - a method for noninvasive assessment of myocardial motion, Radiology 169 (1) (1988) 59–63.

[17] C. Petitjean, N. Rougon, P. Cluzel, Assessment of myocardial function: A review of quantification methods and results using tagged MRI, Journal of Cardiovascular Magnetic Resonance 7 (2) (2005) 501–516.

[18] L. Axel, S. Chung, T. Chen, Tagged MRI analysis using gabor filters, in: Biomedical Imaging: From Nano to Macro, 4th IEEE International Symposium on (ISBI), 2007, pp. 684–687.

[19] A. Histace, Détections et suivis robustes de structures dans des séquences d'images : application à l'IRM cardiaque marquée, Ph.D. thesis, Université d'Angers (2004).

[20] B. Frieden, Fisher information as a measure of time, Astrophysics and Space Sciences 244 (1996) 387–391.

[21] R. Fisher, Philosophical Transactions of the Royal Society of London 222 (1922) 309.

[22] A. Histace, V. Courboulay, M. Ménard, Selective image diffusion for oriented pattern extraction, in: 4th International Conference on Informatics in Control, Automation and Robotics (ICINCO), 2007, pp. 270–274.

[23] S. Zhang, M. Douglas, L. Yaroslavsky, R. Summers, V. Dilsizian, L. Fananapazir, S. Bacharach, A fourier based algorithm for tracking SPAMM tags in gated magnetic resonance cardiac images, Medical Physics 32 (8) (1996) 1359–1369.

[24] W. Kerwin, N. Osman, J. Prince, Handbook of Medical Imaging, Academic Press, San Diego CA, 2000, Ch. 24, pp. 375–391.

[25] A. Rao, R. Jain, Computerized flow field analysis: Oriented texture fields, Transactions on pattern analysis and machine intelligence 14 (7).

[26] B. Tremblais, B. Augereau, M. Leard, Multiscale approach for the extraction of vessels, in: Proceedings of SPIE Medical Imaging, Vol. 5032, 2003, pp. 1331–1345.

[27] A. Histace, B. Matuszewski, Y. Zhang, Segmentation of myocardial boundaries in tagged cardiac MRI using active contours: a gradient-based approach integrating texture analysis, International Journal of Biomedical Imaging, Vol. 2009, 2009, Article ID 983794, 8 pages.

[28] J. Weickert, Scale-space properties of nonlinear diffusion filtering with a diffusion tensor, Report 110, University of Kaiserslautern, Laboratory of Technomathematics 67653 Kaiserslautern Germany (1994).